激光快速成形 TA15 钛合金氩弧焊接头组织及力学性能

杜博睿， 田象军， 王华明
（北京航空航天大学 材料科学与工程学院，北京 100191）

摘 要： 对激光快速成形 TA15 钛合金与轧制 TA15 钛合金薄板进行了氩弧焊接试验，观察分析了焊接接头各区域组织特征，测试了焊接接头各区域的显微硬度以及室温拉伸性能. 结果表明，激光快速成形件与轧制薄板氩弧焊焊缝凝固组织是具有粗大片状 $\alpha+\beta$ 组织特征外延定向生长的柱状晶. 轧制件对焊接热影响敏感性强，热影响区晶粒发生严重长大现象，激光成形件靠近焊缝热影响区晶粒转变为等轴晶，距焊缝较远的热影响区仍保持柱状晶. 激光成形件热影响区硬度最高，焊缝区及轧制件热影响区的硬度最低. 焊接接头抗拉强度低于母材，塑性与轧制件相当，断裂位置位于轧制件热影响区.

关键词： 钛合金；激光快速成形；氩弧焊；组织；力学性能
中图分类号： TG444.74 **文献标识码：** A **文章编号：** 0253－360X(2013)11－0065－04

杜博睿

0 序 言

目前在现有航空制造业中，相对于传统的机械连接工艺，焊接技术的应用越来越广泛. 激光快速成形钛合金与传统成形钛合金显微组织上存在很大差异，因而焊接性能也应有所不同. 氩弧焊作为一种广泛应用的焊接方法，具有成本低、工艺操作灵活的优点，且尤为适合制备复杂零件. 对于传统成形钛合金的焊接特性研究已较为成熟[1,2]，而激光快速成形钛合金焊接性能的相关研究还相对较少[3]. 文中对比研究了激光快速成形 TA15 钛合金与轧制 TA15 钛合金氩弧焊接接头组织特征及变化规律，并对接头显微硬度和力学性能进行了测试，为激光快速成形 TA15 钛合金的焊接奠定技术基础.

1 试验方法

试验试样选用激光快速成形 TA15 钛合金与冷轧 TA15 钛合金薄板，首先用线切割将激光快速成形 TA15 毛坯件切成 3 mm 厚薄板，再通过氩弧焊与 3 mm 厚的冷轧薄板焊接在一起. 焊接方向垂直于激光成形件沉积增高方向和冷轧薄板轧制方向. 试样在焊前加工 V 形坡口，使用丙酮清洗表面后烘干. 为确保试样焊透，并通过增大热输入加强焊接热输入对两种材料的影响，对试样进行正反双面焊. 焊接试验设备为 Fronius TPS2700 MIG 气体保护焊机，焊丝采用直径为 1.2 mm 的 TA15 钛合金焊丝，焊接电流为 200～300 A，电弧电压为 20～30 V，焊接过程在纯度为 99.99% 的氩气箱内进行. 焊后对焊缝处用 X 射线检验，未发现明显缺陷.

利用 Olympus BX51M 型光学显微镜及 CS3400 型扫描电镜观察焊接接头组织. 利用 FM-800 型显微硬度仪测定焊接接头显微硬度分布，载荷为 5 N，加载时间为 10 s. 焊接好的试样加工成非标准板材拉伸试样，在 INSTRON5565 型微机控制电子万能试验机上测试室温拉伸性能.

2 显微组织分析

2.1 母材组织

图 1 为激光快速成形 TA15 和轧制 TA15 宏观组织形貌，激光快速成形 TA15 宏观组织为贯穿多个熔覆层外延生长的柱状晶，柱状晶生长方向基本垂直于基材和扫描方向，晶粒宽度约为 1～3 mm. 轧制态 TA15 宏观组织为沿轧制流动方向生长的流线型纤维状织构.

收稿日期： 2012－11－25
基金项目： 国家重点基础研究发展计划资助项目(2011CB606305)

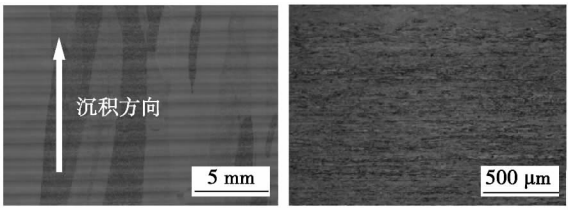

(a) 激光快速成形 TA15 (b) 轧制TA15

图 1 激光快速成形 TA15 和轧制 TA15 宏观组织形貌

Fig. 1 Macrostructure of laser melting deposited TA15 and rolled TA15

2.2 焊缝区凝固组织

图 2 为经过正反双面氩弧焊接后垂直于焊接方向的接头纵截面形貌. 焊接接头两端凝固组织为以激光成形件和轧制件母材半熔化晶粒为基底外延定向生长的柱状晶. 由于钛合金导热系数小,对过热非常敏感,在焊接热循环的作用下,熔池边界半熔化晶粒的尺寸变得十分粗大,使外延生长的 β 柱状晶也十分粗大. β 柱状晶的生长方向是沿着最大散热方向进行的,可以清晰的看到 β 柱状晶由熔合线向焊缝表面生长. 第二道焊缝(反面)是以第一道焊缝(正面)底部未熔化的晶粒为基底外延定向生长的.

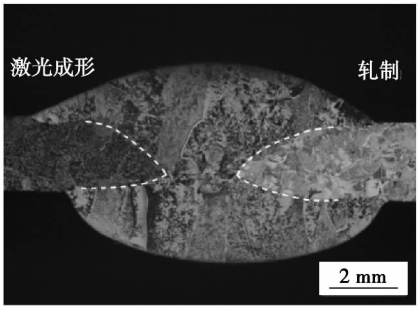

(a) 宏观形貌

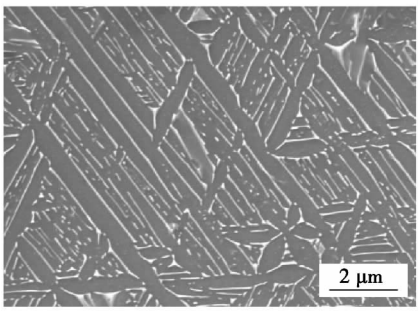

(b) 微观形貌

图 2 焊接接头纵截面宏观和微观组织形貌

Fig. 2 Macro and microstructure of longitudinal section of welding joint

为了对比说明焊接热输入对两种母材热影响的差异,所采用的氩弧焊焊接热输入大,焊接速度低,高温停留时间长,冷却速度慢,焊缝凝固时并不发生马氏体相变[4,5]. 焊缝凝固区显微组织为明显的片状 $\alpha+\beta$ 组织特征,熔池冷却速率较慢,导致产生的过冷度较小,α 相析出时优先在晶界上形核,β 相晶粒具有完整的 α 相晶界,由晶界向晶内生长,且具有一定的方向性,在原始 β 相晶粒内形成集束,在同一集束内的 α 相彼此平行成同一取向. 而在 β 相晶粒内部,针状 α 相沿不同方向析出,由于熔池高温停留时间较长,使得针状 α 相充分长大,不同的相相遇后停止长大,形成粗大的片状 α 相组织,第一道焊缝与第二道焊缝凝固组织没有明显差异.

2.3 激光成形件热影响区组织

图 3 为激光成形件热影响区纵截面的宏观形貌. 经过两次热循环后,激光成形件热影响区靠近焊缝部分的原始 β 相柱状晶转变为等轴晶,晶粒尺寸达到 1 mm 左右. 有研究表明,激光快速成形钛合金组织对激光深熔焊的热影响不敏感,焊缝热影响区 β 相晶粒无长大现象[6]. 相比激光深熔焊氩弧焊的热输入较大,靠近焊缝的热影响区温度达到 β 相转变点以上较高处,以原始 β 相作为形核基底,β 相逐渐增加,α 相逐渐消失,当不同位相的 β 长大相遇后形成晶界,在一定时间的高温热作用下,小晶粒继续长大并不断合并成大晶粒,最终由原来的柱状晶转变为等轴晶.

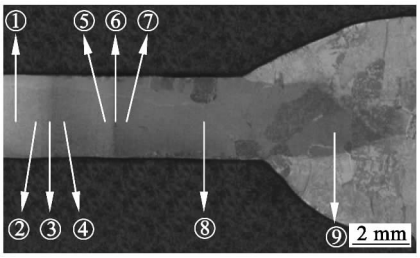

图 3 激光成形件热影响区宏观形貌

Fig. 3 Macro morphology of heat affected zone of laser melting deposited TA15

图 4 为对应图 3 中①~⑨各区域的显微组织形貌,①区域为离焊缝较远的母材组织,经过第一道焊接热输入后. ②区域受热影响加热到两相区,冷却过程中沿初生 α 相边界析出细小次生 α 相. ③区域加热到两相区上部,次生 α 相从残余 β 相中析出. 焊缝与③区域之间的组织全部 β 相化,冷却下来形成细长片状组织. 第二道焊接热输入小于第一道,受热影响的区域变短. 受第一次热影响而转变为细长片状组织的⑤区域,在受第二次热影响时,温度升高到两相区,初生 α 相层粗化,体积分数减小,冷却

过程中次生 α 相由初生 α 相边界形核向 β 相内生长. ⑥区域温度升高到两相区上部，同③区域组织特征大致相同. 焊缝与⑦区域之间的组织受热全部转变为 β 相，柱状晶(⑧区域)以及等轴晶(⑨区域)内组织均为细长层片状组织.

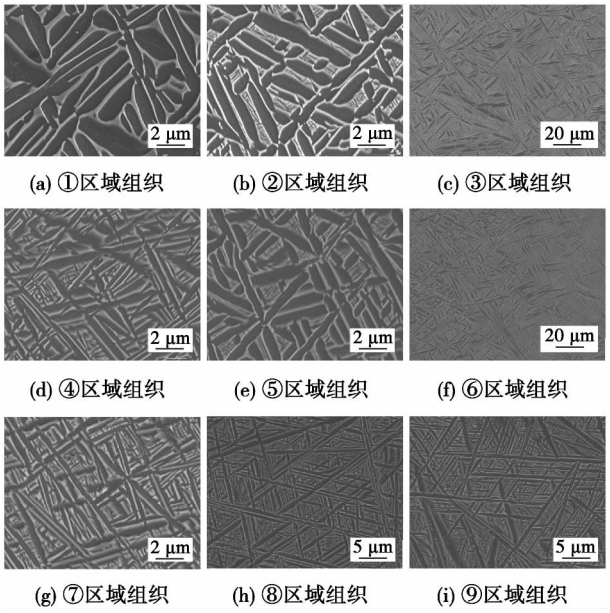

图 4　激光成形 TA15 热影响区各区域显微组织形貌

Fig. 4　Microstructure of different positions in heat affected zone of laser melting deposited TA15

2.4　轧制件热影响区组织

图 5 为焊接接头轧制件热影响区宏观形貌. 相对于激光成形件，轧制件内部存在更大的形变储存能，β 相晶粒在焊接的热影响下更易于长大. 靠近焊缝的区域，β 相晶粒受焊接热作用高温停留的时间较长，原始组织再结晶形核后充分长大，晶粒尺寸达到 300 μm，形成粗晶区. 随着离焊缝距离增加，受焊接热作用的时间缩短，晶粒长大的程度减小，靠近母材区域的晶粒尺寸降至 50 μm 以下，形成细晶区. 接近母材的热影响区，受焊接热作用的温度刚好达到再结晶温度，因轧制形成的形变织构开始发生回复再结晶，形成不完全再结晶区(过渡区).

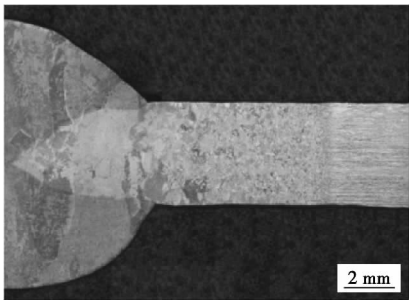

图 5　轧制 TA15 热影响区宏观形貌

Fig. 5　Macrostructure of heat affected zone of rolled TA15

图 6 为激光快速成形及轧制 TA15 氩弧焊焊接接头组织示意图. 从图 6 中可以看出，焊缝凝固组织均以母材半熔化晶粒为基底外延定向生长的柱状晶. 经过两次焊接热循环后激光成形件靠近焊缝的热影响区 β 相柱状晶转变为等轴晶，远离焊缝的区域保持尺寸不变. 而轧制件对焊接热敏感性较强，β 相晶粒发生长大现象，且离焊缝越近长大现象越严重.

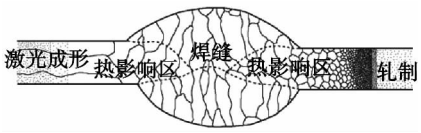

图 6　焊接接头组织示意图

Fig. 6　Schematic illustration of weld joint

3　力学性能分析

3.1　显微硬度

对接头横截面水平方向进行了显微硬度测试，分布曲线如图 7 所示. 接头各个区域中，激光成形件热影响区硬度最高，激光成形件母材硬度次之，轧制件母材硬度低于激光成形件，而焊缝区及轧制件热影响区的硬度最小. 从硬度分布图可以看出，相比轧制 TA15，激光成形 TA15 的硬度受焊接热作用影响较小.

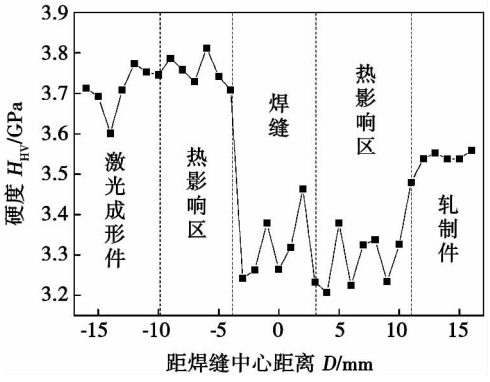

图 7　焊接接头各区域显微硬度分布

Fig. 7　Distribution of microhardness in welding joint

3.2　室温拉伸性能

激光快速成形 TA15 与轧制 TA15 钛合金氩弧焊接接头及其母材的室温拉伸性能结果如表 1 所示.

表 1 氩弧焊接接头及母材拉伸性能

Table 1 Tensile properties of argon-arc welding joint and base metal

测试对象	抗拉强度 R_m/MPa	屈服强度 R_{eL}/MPa	断后伸长率 A(%)	断面收缩率 Z(%)	断裂位置
激光成形母材	986.2	849.5	8.3	25.8	—
轧制母材	1 026.7	926.7	11.2	26.1	—
焊接接头	936.2	801.8	11.1	27.3	轧制热影响区

焊接接头拉伸试样在试验过程中均断裂在轧制件热影响区. 抗拉强度略低于母材,相比激光成形母材和轧制母材分别下降了 5.0% 和 8.8%. 由此可以得出,在相同的焊接条件下,激光快速成形件接头抗拉强度高于轧制件.

4 结 论

(1) 激光快速成形 TA15 与轧制薄板 TA15 氩弧焊焊缝凝固组织是以母材半熔化的晶粒为基底外延定向生长的粗大 β 相柱状晶,显微组织为具有粗大片状 $\alpha+\beta$ 组织.

(2) 轧制件对焊接热影响敏感性强,热影响区发生再结晶及长大,且距焊缝越近晶粒长大越严重. 激光成形件靠近焊缝热影响区转变为等轴晶,离焊缝较远的热影响区仍保持柱状晶.

(3) 激光成形件热影响区硬度最高,焊缝及轧制件热影响区硬度最低.

(4) 焊接接头抗拉强度低于两种母材,塑性与轧制件相当; 断裂位置位于轧制件热影响区.

参考文献:

[1] 《中国航空材料手册》编辑委员会. 中国航空材料手册,钛合金铜合金 [M](2 版). 北京: 中国标准出版社, 2002.

[2] 吴 巍, 高洪明, 程广福, 等. 细晶粒钛合金热影响区晶粒长大规律 [J]. 焊接学报, 2008, 29(10): 57 - 61.
Wu Wei, Gao Hongming, Cheng Guangfu, *et al*. Grain growth in heat affected zone of fine grained titanium alloy [J]. Transactions of the China Welding Institution, 2008, 29(10): 57 - 61.

[3] 李 旭, 刘 栋, 汤海波, 等. 激光熔化沉积 TC17 钛合金光纤激光焊接特性 [J]. 中国激光, 2012, 39(1): 0103010.
Li Xu, Liu Dong, Tang Haibo, *et al*. Fiber laser welding characteristics of laser melting deposited TC17 alloy [J]. Chinese Journal of Lasers, 2008, 39(1): 0103010.

[4] 姚 伟, 巩水利, 陈 俐. 钛合金激光焊接接头的组织和力学性能 [J]. 焊接学报, 2006, 27(2): 69 - 72.
Yao Wei, Gong Shuili, Chen Li. Microstructures and mechanical properties of titanium alloy laser beam welding joints [J]. Transactions of the China Welding Institution, 2006, 27(2): 69 - 72.

[5] 吴 巍, 程广福, 高洪明, 等. TC4 合金 TIG 焊接头组织转变与力学性能分析 [J]. 焊接学报, 2009, 30(7): 81 - 84.
Wu Wei, Cheng Guangfu, Gao Hongming, *et al*. Microstructure transformation and mechanical properties of TC4 alloy joints welded by TIG [J]. Transactions of the China Welding Institution, 2009, 30(7): 81 - 84.

作者简介: 杜博睿,男,1988 年出生,硕士研究生. 主要从事钛合金焊接、钛合金激光快速成形方面的研究. Email: buaadbr@ gmail.com

通讯作者: 田象军,男,讲师. Email: tianxj_n@ buaa. edu. cn

point of Al-Si moves to the Si side. It can be found that the phases in Al-Si-Zn brazed 6061 aluminum joint are α-Al, η-Zn, and Si particles, and the phases in Al-Si-Zn-Cu-P brazed seam are α-Al, η-Zn, fine Si particles, AlP phase.

Key words: modification; brazing; 6061 aluminum alloy; Si

Design of high power underwater laser cutting nozzle

XU Liang[1], WANG Wei[1], LI Xiaoyu[1], XU Yujun[1], LIU Shaowei[2] (1. Harbin Welding Institute, China Academy of Machinery Science and Technology, Harbin 150028, China; 2. Shenyang Xinle Aerospace Co., Ltd., Shenyang 110034, China). pp 57 - 60

Abstract: According to the principle of the laser spot size requirement and the design principle of Laval nozzle, the part of stable section, contraction section, throat section and expansion section of the nozzle were designed. The size of stable section is mainly limited by the overall size of the laser cutting gun. Contraction section is used to connect the stable period and the throat section by using tangent arc transition. In order to ensure the laser go smoothly through the throat, throat diameter must be greater than the laser spot diameter. Expansion section adopts linear expansion method, in view of the cutting seam width limit, divergence angle should not be too large. According to the design size, the supersonic Laval nozzle was manufactured, the jet velocity and stiffness of oxygen flow was improved. In underwater laser cutting experiment, using the local drainage method and larger oxygen flow, 30 mm thick carbon steel plate was cut smoothly. Compared with the convergent nozzle, the cutting effect of the supersonic nozzle has been obviously improved

Key words: underwater; cutting; laser; nozzle

Effect of rare earth Ce on microstructure and properties of Zn-22Al filler metal

WANG Bo[1], LIU Han[1], XUE Songbai[1], LI Yang[1], LOU Jiyuan[2], LOU Yinbin[2] (1. College of Materials Science and Technology, Nanjing University of Aeronautics and Astronautics, Nanjing 210016, China; 2. Zhejiang Xinrui Welding Material Co., Ltd., Shengzhou 312452, China). pp 61 - 64

Abstract: The effects of the rare earth Ce on the resistivity, melting temperature, spreadability, microstructure of Zn-22Al filler metal and shear strength of brazed joints were studied. The results indicated that the addition of Ce has little effect on the resistivity and the melting temperature of the filler metal. But with the addition of Ce, the spreadability is significantly improved, the microstructure is refined obviously. It has been found that Ce can improve the shear strength of Cu/Al joint notablely. When the content of Ce is 0.05%, the spread area of filler metal on Al and Cu substrates reached maximum values, respectively, which are 21.4% and 11.6% higher than those of Zn-22Al alloy respectively. Moreover, the shear strength of Cu/Al joint brazed with Zn-22Al-0.05Ce reaches the peak value of 91.3 MPa, which is improved by 30.3% compared with the joint brazed with Zn-22Al alloy. However, with the addition of excessive amount of Ce, some brittle Ce-bearing phases appear in the microstructure and their sizes increase, and the spreadability of filler metal and shear strength of Cu/Al joint deteriorate significantly.

Key words: rare earth Ce; Zn-Al filler metal; spreadability; microstructure; mechanical properties

Microstructure and mechanical properties of MIG welded joint of laser melting deposited TA15 titanium alloy

DU Borui, TIAN Xiangjun, WANG Huaming (School of Material Science and Engineering, Beihang University, Beijing 100191, China). pp 65 - 68

Abstract: Laser melting deposited (LMD) TA15 and rolled TA15 were welded by argon arc welding. The microstructure and phase constitution of the welded joint were studied by optical microscopy and scanning electron microscopy. The microhardness and mechanical properties of the welded joint were tested. The results indicate that the weld zone (WZ) mainly consists of columnar crystals with thick lamellar structure which epitaxially grow from the substrates. The grains in heat affected zone (HAZ) of rolled TA15 grow seriously because of its sensitivity to heat. The columnar grains in HAZ near weld zone of LMD TA15 turn into equiaxial grains. The microhardness of HAZ of LMD TA15 is the highest, while the WZ and HAZ of rolled TA15 is the lowest. The tensile strength of the welded joint is lower than that of both base metals, but the plasticity corresponds to the rolled TA15. Fracture position locates in the HAZ of rolled TA15.

Key words: titanium alloy; laser melting deposition; argon-arc welding; microstructure; mechanical properties

Fatigue life prediction of transverse cross welded joint based on different S - N curve

FAN Wenxue[1,2], CHEN Furong[1], XIE Ruijun[1], GAO Jian[1] (1. School of Materials Science and Engineering, Inner Mongolia University of Technology, Hohhot 010051, China; 2. School of Mining Institute, Inner Mongolia University of Technology, Hohhot 010051, China). pp 69 - 72

Abstract: Three kinds of S - N curves including experimental S - N curve, experience S - N curve and standard S - N curve were established by MSC. Fatigue software. The effects of residual stress, average stress and joint shape were considered. And these curves were revised according to the related criterion and used to predict the fatigue life of Q235B cross-shaped welded joint. The results show that, the fatigue damage locations of welded joint is consistent with that of experiment by S - N curve method based on MSC. Fatigue. The deviation is 7.9%-28% between the prediction values of experiment S - N curve and that of standard S - N curve. The deviation is 3.3%-19% between the prediction values of experiment S - N curve and that of experience S - N curve. The prediction values of experience S - N curve are higher than that of experiment S - N curve and that of standard S - N curve is more conservative.

Key words: cross welded joint; fatigue life; finite element analysis; S - N curve

Filler wire melting dynamics during laser beam welding with filler wire

LIU Hongbing[1], TAO Wang[2,3], CHEN Jie[1], YANG Zhibin[2], CHEN Lei[1], ZHAN Xiaohong[1], LI Liqun[2] (1.